IEEE Access
Multidisciplinary | Rapid Review | Open Access Journal

Received February 13, 2020, accepted March 9, 2020, date of publication March 13, 2020, date of current version March 25, 2020.

Digital Object Identifier 10.1109/ACCESS.2020.2980677

Improving the Shearer Positioning Accuracy Using the Shearer Motion Constraints in Longwall Panels

SHIJIA WANG AND SHIBO WANG
School of Mechanical and Electronic Engineering, China University of Mining and Technology, Xuzhou 221116, China
Intelligent Mining Equipment Collaborative Innovation Center, China University of Mining and Technology, Xuzhou 221116, China

Corresponding author: Shibo Wang (wangshb@cumt.edu.cn)

This work was supported in part by the Funds of the Natural Science Foundation of China under Grant U1610251 and Grant 51874279, and in part by the Priority Academic Program Development of Jiangsu Higher Education Institutions (PAPD).

ABSTRACT The shearer positioning method with an inertial navigation system (INS) is feasible in a longwall mining face. However, INS error greatly increases with time, which reduces the shearer positioning accuracy. This study aims to improve the shearer positioning accuracy using the shearer motion constraints. Firstly, according to the longwall mining method, two constraints on the shearer velocity and position were obtained. Then, velocity constraint information and position constraint information were modeled to obtain the observation equations in the filter. In order to improve the shearer positioning accuracy, an information filter was utilized to integrate the velocity constraint information and position constraint information. Finally, an experiment was performed to validate the effectiveness of the proposed algorithm. The result showed that the shearer positioning accuracy improved by 56% in the east and 54% in the north.

INDEX TERMS Shearer positioning, inertial navigation system, information filter.

I. INTRODUCTION

Longwall mining is the predominant method applied in the underground mine at present. Three types of equipment working in a longwall mining face are a shearer, an armored face conveyor (AFC), and a roof support system, as shown in Fig. 1. The shearer moves back and forth along a rail associated with the AFC, while the roof support system supports the coal seam roof. Traditionally, these three types of equipment are operated manually. This not only reduces the mining productivity, but also exposes the worker to the hazardous environment. Improving mining productivity and protecting worker safety are goals constantly pursued by the coal industries [1], [2]. The automatic mining technology has shown significant potential to achieve these goals by providing the shearer positioning, face alignment, horizontal control, remote control, and so on [3]–[5]. Among these technologies, shearer positioning is the basis of the others. Because there is no Global Position System (GPS) signal in the underground environment, shearer positioning technology based on the inertial navigation system (INS) is a feasible method [6]–[8]. The INS achieves high short-time accuracy and good autonomy. However, the major disadvantage is the accumulated error over time [9], [10]. In the underground coal mine, the positioning technology based on INS faces the problem of rapid error growth. To solve this problem, researchers proposed several methods to aid INS for the underground mining equipment.

Fan *et al.* [11] developed the wireless sensor network (WSN) to aid the shearer INS. Four anchor nodes were installed on the roof support system and the mobile node was installed on the shearer body. The result showed that the position error was less than 0.2 m within 1200 s. However, the disadvantage was that the position coordinates of anchor nodes could not be accurately determined because the roof support system moved forward intermittently. Xie *et al.* [12] used tilt sensors installed on the shearer body and AFC to aid INS for the shearer and AFC positioning. The experiment demonstrated that the position error was less than 0.38 times the middle trough length and the positioning accuracy improved 21%. However, this method only obtained the one-dimensional position of the shearer, which couldn't meet the need of three-dimensional positioning. Dunn *et al.* [13], [14] used a Doppler radar to aid INS. The

The associate editor coordinating the review of this manuscript and approving it for publication was Chao Tan.

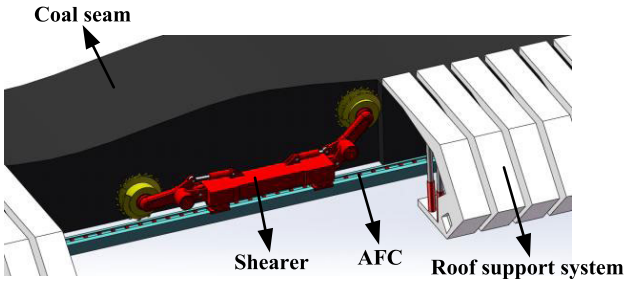

FIGURE 1. The diagram of the shearer, AFC, and roof support system [18].

Doppler radar measured the relative speed between the continuous miner and the ground, which was applied to correct the INS speed error. However, the measurement accuracy and stability were greatly affected by the surrounding environment.

The authors of this paper developed a shearer positioning system based on an INS and an axial encoder (Fig. 2(b)), which used the dead reckoning algorithm to obtain the shearer moving trajectory [15]. According to the previous research [16], [17], the integrated navigation of the INS and the axial encoder had the better positioning accuracy compared with the INS. The INS, providing the attitude angles (heading, pitch, and roll), was embedded in the shearer body, and the axial encoder, providing the velocity value, was connected to the haulage unit of the shearer, as shown in Fig. 2(a). Because of the INS accumulated error, it was necessary to have other ways to aid the shearer INS. Therefore, this study used the shearer motion constraints to aid the INS to improve the positioning accuracy.

The remainder of this paper is organized as follows. First, the article analyzed the longwall mining method and obtained the motion constraints including the velocity constraint and the position constraint. The velocity observation information and position observation information were modeled to obtain the observation equations. Then, an information filter algorithm integrating the velocity observation information and position observation information was used to improve the shearer positioning accuracy. Finally, an experiment was conducted to validate the effectiveness of the information filter algorithm.

II. LONGWALL MINING METHOD

Longwall mining is widely applied and is an efficient mining method for extracting a high percentage of coal from the underground mine. A coal seam is usually divided into several longwall panels by excavating roadways as the boundaries shown in Fig. 3(a). A longwall panel is generally 300 m wide, 5000 m long, and 1.2-8.0 m thick. The shearer, AFC, and roof support system are installed across the back of the panel, creating a longwall face (Fig. 3(b)) [19], [20].

The shearer reciprocates along a rail associated with the AFC, cutting a 0.8 m-wide slice of coal from the coal seam.

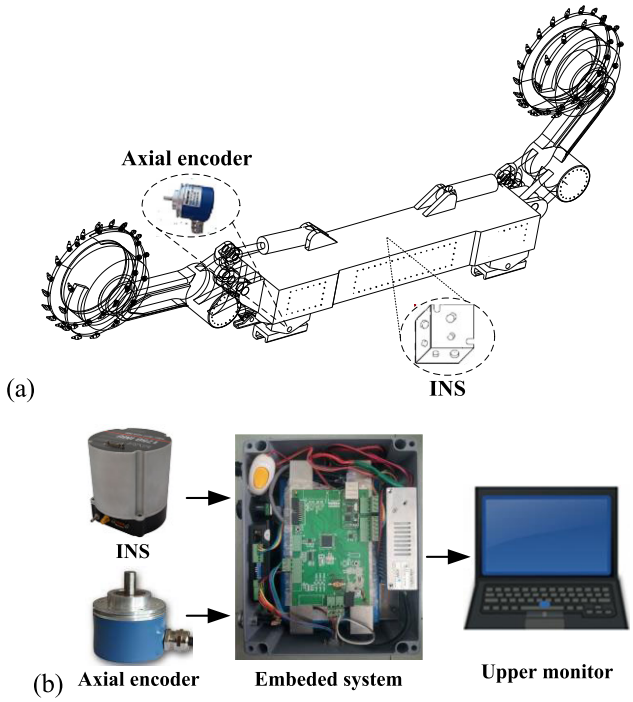

FIGURE 2. The diagram of (a) the installation position of the INS and the axial encoder and (b) the shearer positioning system.

The rail limits the shearer motion along the lateral and vertical directions (X-axis and Z-axis in the shearer coordinate system shown in Fig. 4). The shearer velocity in the X-axis and Z-axis, perpendicular to the Y-axis, should be zero. This can be used as a velocity constraint to improve the shearer positioning accuracy.

As shown in Fig. 4, when the shearer cuts the coal seam, a part of the AFC, behind the shearer, is progressively pushed towards the coal seam by large hydraulic push arms attached to the roof support system for the next cutting cycle. A cutting cycle refers to the process in which the shearer moves the whole length of the longwall face. In Fig. 4, the shearer is moving during the second cutting cycle. The displacement sensor fixed inside the push arm measures the advancing displacement of each section of the AFC. The shearer positioning system shown in Fig. 2(b) measures the AFC position when the shearer runs along the AFC [21], [22]. According to the AFC measured position and the advancing displacements, the AFC position during the next cutting cycle can be predicted, which will be used as a position constraint to improve the shearer positioning accuracy.

According to the above analysis, the motion constraints on the shearer velocity and position were obtained. The velocity constraint and the position constraint can be understood as two observations. Based on the multi-observations information fusion method, an information filter was used to integrate the velocity observation and the position observation in this study.

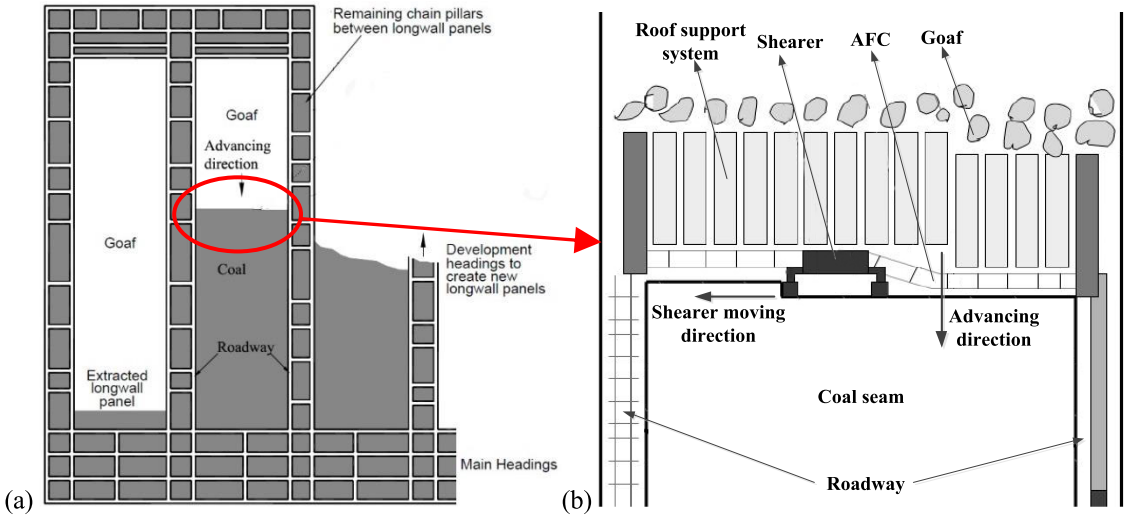

FIGURE 3. Typical plan view of (a) a coal mine and (b) a longwall face [23].

III. STATE EQUATION

The state equation of the filter is derived from the INS error equation, which is often used in the integrated navigation system [25], [26]. The error equation is derived from the calculation principle of navigation parameters, and it reflects the essential property of the INS error to some extent. The equations of position error, velocity error, and attitude angle error [9], [27], [28] are given as follows,

$$\begin{cases} \dot{\delta L} = \dfrac{1}{R_n + h}\delta V_N + (-\dfrac{V_N}{(R_n + h)^2})\delta h \\ \dot{\delta\lambda} = \dfrac{1}{(R_e + h)\cos L}\delta V_E + \dfrac{V_E \tan L}{(R_e + h)\cos L}\delta L \\ +(-\dfrac{V_E}{(R_e + h)^2 \cos L})\delta h \\ \dot{\delta h} = \delta V_U \end{cases} \tag{1}$$

$$\begin{cases} \dot{\delta V_E} = (2\omega_{ie}\sin L + \dfrac{V_E \tan L}{R_e + h})\delta V_N + \dfrac{V_N \tan L - V_U}{R_e + h}\delta V_E \\ +(-2\omega_{ie}\cos L - \dfrac{V_E}{R_e + h})\delta V_U + \dfrac{V_E V_U - V_N V_E \tan L}{(R_e + h)^2}\delta h \\ +(2(\omega_{ie} V_N \cos L + \omega_{ie} V_U \sin L) + \dfrac{V_N V_E \sec^2 L}{R_e + h})\delta L \\ +f_N \delta\phi_U - f_U \delta\phi_N + \eta_E \\ \dot{\delta V_N} = (-\dfrac{V_U}{R_n + h})\delta V_N + (-2\omega_{ie}\sin L - \dfrac{2V_E \tan L}{R_e + h})\delta V_E \\ +(-\dfrac{V_N}{R_n + h})\delta V_U + \dfrac{V_N V_U + V_E^2 \tan L}{(R_e + h)^2}\delta h \\ +(-2\omega_{ie} V_E \cos L - V_N \cos L - \dfrac{V_E^2 \sec^2 L}{R_e + h})\delta L \\ +f_U \delta\phi_E - f_E \delta\phi_U + \eta_N \\ \dot{\delta V_U} = \dfrac{2V_N}{R_n + h}\delta V_N + (2\omega_{ie}\cos L + \dfrac{2V_E}{R_e + h})\delta V_E \\ +(-\dfrac{V_E^2}{(R_e + h)^2} - \dfrac{V_N^2}{(R_n + h)^2})\delta h + (-2\omega_{ie} V_E \sin L)\delta L \\ +f_E \delta\phi_N - f_N \delta\phi_E + \eta_U \end{cases} \tag{2}$$

$$\begin{cases} \dot{\delta\phi_E} = (\omega_{ie}\sin L + \dfrac{V_E \tan L}{R_e + h})\delta\phi_N + (-\omega_{ie}\cos L \\ -\dfrac{V_E}{R_e + h})\delta\phi_U + (-\dfrac{1}{R_n + h})\delta V_N + \dfrac{V_N}{(R_n + h)^2}\delta h + \varepsilon_E \\ \dot{\delta\phi_N} = (-\omega_{ie}\sin L - \dfrac{V_E \tan L}{R_e + h})\delta\phi_E + (-\dfrac{\delta V_N}{R_n + h})\delta\phi_U \\ +\dfrac{1}{R_e + h}\delta V_E + (-\omega_{ie}\sin L)\delta L + \dfrac{V_E}{(R_e + h)^2}\delta h + \varepsilon_N \\ \dot{\delta\phi_U} = (\omega_{ie}\cos L + \dfrac{V_E}{R_n + h})\delta\phi_E + (\dfrac{V_N}{R_n + h})\delta\phi_N \\ +(\omega_{ie}\cos L + \dfrac{\delta V_E \sec^2 L}{R_e + h})\delta L + \dfrac{\tan L}{R_e + h}\delta V_E + \varepsilon_U \end{cases} \tag{3}$$

where L, λ, and h are the latitude, longitude, and altitude, whose errors are defined as δL, $\delta\lambda$, and δh, respectively; V_E, V_N, and V_U are the velocity values in the east-north-up (ENU) coordinate system, δV_E, δV_N, and δV_U are its errors, respectively; $\delta\Phi_E$, $\delta\Phi_N$, and $\delta\Phi_U$ are the platform orientation errors in the east, north, and up, respectively; R_n and R_e are the curvature radii along the meridian and parallel, respectively; ω_{ie} is the angular velocity of the rotation of the earth; f_E, f_N, and f_U are the specific forces in the east, north, and up, respectively; η_E, η_N, and η_U are the accelerometer biases in the ENU coordinate system; ε_E, ε_N, and ε_U are the gyroscope drifts in the ENU coordinate system.

In this study, the state vector is given by,

$$\boldsymbol{X} = [\delta L\ \delta\lambda\ \delta h\ \delta V_E\ \delta V_N\ \delta V_U\ \delta\phi_E\ \delta\phi_N\ \delta\phi_U]^T \tag{4}$$

The equations of the position error, velocity error and attitude angle error can be rewritten as a matrix form as follows,

$$\dot{\boldsymbol{X}} = \boldsymbol{A}\boldsymbol{X} + \boldsymbol{B}\boldsymbol{u} \tag{5}$$

where $\boldsymbol{A}$ is obtained according to Eq. (1), (2), and (3); $\boldsymbol{B}$ is the distribution matrix of processing the white noise; $\boldsymbol{u}$ is the white noise vector. Therefore, the state equation is obtained

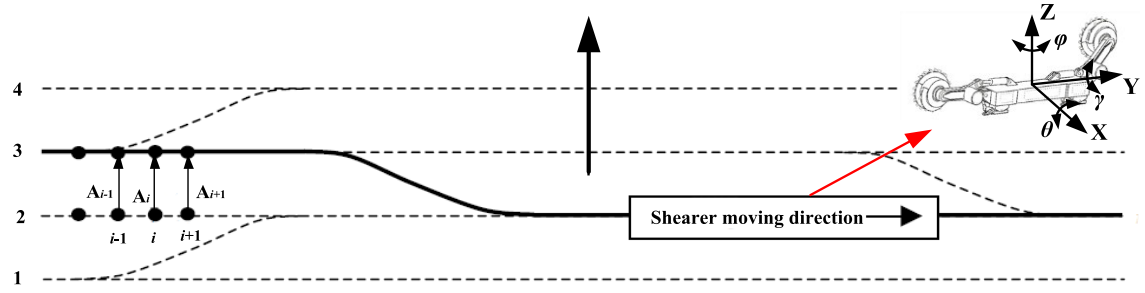

FIGURE 4. The diagram of the AFC profile when the shearer moves [24].

as follows,

$$\boldsymbol{X}(k\,|k-1) = \boldsymbol{F}(k\,|k-1)\boldsymbol{X}(k-1) + \boldsymbol{W}(k-1) \quad (6)$$

where $\boldsymbol{F}$ is the state transition matrix, which satisfies $\boldsymbol{F}$=exp($\boldsymbol{A}Ts$); T_S is the computation period; $\boldsymbol{W}$ is the state noise.

IV. OBSERVATION EQUATIONS

A. VELOCITY OBSERVATION EQUATION

According to the velocity constraint described in Section II, the shearer velocity in both the X-axis and Z-axis (shown in Fig. 4) should be zero. However, the velocity (V_{ox} and V_{oz}) measured by the INS in these two axes is not equal to zero in practice, which is defined as the velocity error (δV_{ox} and δV_{oz}). The velocity error is transformed into the velocity observation vector by Eq. (7).

$$\begin{bmatrix} \delta V_{OE} \\ \delta V_{ON} \\ \delta V_{OU} \end{bmatrix} = \boldsymbol{C}_{\boldsymbol{b}}^{\boldsymbol{n}} \begin{bmatrix} \delta V_{ox} \\ 0 \\ \delta V_{oz} \end{bmatrix} \quad (7)$$

where $\boldsymbol{C}_{\boldsymbol{b}}^{\boldsymbol{n}}$ is the direction cosine matrix (DCM) as (8), as shown at the bottom of the next page, which consists of heading angle (θ), pitch angle (φ), and roll angle (γ).

Therefore, the velocity observation vector is,

$$\boldsymbol{Z}_V = [\delta V_{OE}\ \delta V_{ON}\ \delta V_{OU}]^T \quad (9)$$

The velocity observation equation in the filter is given by,

$$\boldsymbol{Z}_V(k) = \boldsymbol{H}_V(k)\boldsymbol{X}(k) + V_{\boldsymbol{V}}(k) \quad (10)$$

where $\boldsymbol{H}_V$ is the transition matrix of velocity observation as (11); $\boldsymbol{V}_V$ is the velocity observation noise.

$$\boldsymbol{H}_V = \begin{bmatrix} 0 & 0 & 0 & 1 & 0 & 0 & 0 & 0 & 0 \\ 0 & 0 & 0 & 0 & 1 & 0 & 0 & 0 & 0 \\ 0 & 0 & 0 & 0 & 0 & 1 & 0 & 0 & 0 \end{bmatrix} \quad (11)$$

B. POSITION OBSERVATION EQUATION

According to the position constraint described in Section II, the AFC position during the next cutting cycle is predicted based on the current AFC position and the advancing displacement. When the shearer moves during the next cutting cycle, the measured AFC position is obtained. The difference between the predicted AFC position and the measured AFC position during the next cutting cycle is called the position error (δP_{OE}, δP_{ON}, and δP_{OU}). The position error is transformed into the position observation vector by (12).

$$\begin{bmatrix} \delta L_P \\ \delta \lambda_P \\ \delta h_P \end{bmatrix} = \begin{bmatrix} (\delta P_{OE})/R_e \\ (\delta P_{ON})/(R_n \cos L) \\ \delta P_{OU} \end{bmatrix} \quad (12)$$

Therefore, the position observation vector is given by,

$$\boldsymbol{Z}_{\boldsymbol{P}} = [\delta L_P \quad \delta \lambda_P \quad \delta h_P]^T \quad (13)$$

The observation equation in the filter is,

$$\boldsymbol{Z}_{\boldsymbol{P}}(k) = \boldsymbol{H}_{\boldsymbol{P}}(k)\boldsymbol{X}(k) + \boldsymbol{V}_{\boldsymbol{P}}(k) \quad (14)$$

where $\boldsymbol{H}_{\boldsymbol{p}}$ is the transition matrix of position observation as (15); $\boldsymbol{V}_{\boldsymbol{P}}$ is the position observation noise.

$$\boldsymbol{H}_{\boldsymbol{P}} = \begin{bmatrix} 1 & 0 & 0 & 0 & 0 & 0 & 0 & 0 & 0 \\ 0 & 1 & 0 & 0 & 0 & 0 & 0 & 0 & 0 \\ 0 & 0 & 1 & 0 & 0 & 0 & 0 & 0 & 0 \end{bmatrix} \quad (15)$$

V. INFORMATION FILTER ALGORITHM FOR SHEARER POSITIONING

A. INFORMATION FILTER ALGORITHM

The information filter is an effective method to estimate the system state in multiple observations system [29], [30]. Compared with the Kalman filter, the information filter has a strong robustness. The structure of the information filter is simple. The information filter has advantage in computing, which makes it suitable for real time system [31], [32].

The key components of the information filter are the information matrix ($\boldsymbol{Y}$) and the information state vector ($\boldsymbol{y}$). The information matrix $\boldsymbol{Y}$ is defined as the inverse of the covariance matrix as,

$$\boldsymbol{Y}(k\,|k) = \boldsymbol{P}^{-1}(k\,|k) \quad (16)$$

where $\boldsymbol{P}(k|k)$ is the covariance matrix.

The information state vector $\boldsymbol{y}$, including the information content, is defined as the product of the information matrix and the state vector as follows,

$$\boldsymbol{y}(k\,|k) = \boldsymbol{Y}(k\,|k)\boldsymbol{X}(k\,|k) \quad (17)$$

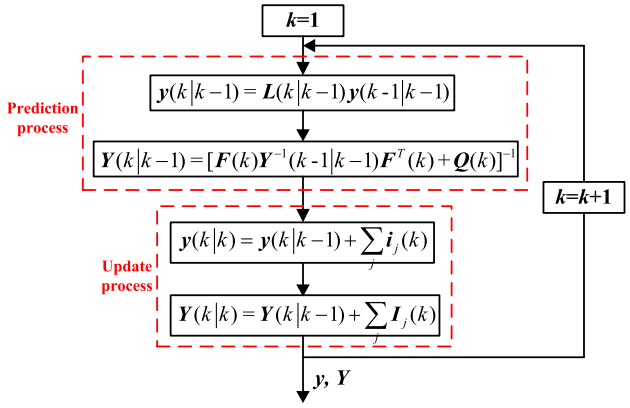

FIGURE 5. The flowchart of the information filter.

The information filter algorithm can be divided into two processes: the prediction process and the update process. The prediction process includes two steps, which are given by,

$$\boldsymbol{y}(k\,|k-1) = \boldsymbol{L}(k\,|k-1)\boldsymbol{y}(k-1\,|k-1) \tag{18}$$

$$\boldsymbol{Y}(k\,|k-1) = [\boldsymbol{F}(k)\boldsymbol{Y}^{-1}(k-1\,|k-1)\boldsymbol{F}^{T}(k) + \boldsymbol{Q}(k)]^{-1} \tag{19}$$

where $\boldsymbol{L}(k|k\text{-}1) = \boldsymbol{Y}(k\text{-}1|k\text{-}1)\boldsymbol{F}(k)\boldsymbol{Y}^{-1}(k\text{-}1|k\text{-}1)$; $\boldsymbol{F}(k)$ is the state transition matrix; $\boldsymbol{Q}(k)$ is the covariance matrix of the state noise. The update process also includes two steps, which are given by,

$$\boldsymbol{y}(k\,|k\,) = \boldsymbol{y}(k\,|k-1\,) + \boldsymbol{i}(k) \tag{20}$$

$$\boldsymbol{Y}(k\,|k\,) = \boldsymbol{Y}(k\,|k-1\,) + \boldsymbol{I}(k) \tag{21}$$

where $\boldsymbol{i}(k) = \boldsymbol{H}(k)^{T}\boldsymbol{R}(k)^{-1}\boldsymbol{Z}(k)$; $\boldsymbol{I}(k) = \boldsymbol{H}(k)^{T}\boldsymbol{R}(k)\boldsymbol{H}(k)$; $\boldsymbol{i}(k)$ is the information observation vector; $\boldsymbol{I}(k)$ is the information observation matrix; $\boldsymbol{H}(k)$ is the observation transition matrix; $\boldsymbol{R}(k)$ is the covariance matrix of the observation noise; $\boldsymbol{Z}(k)$ is the observation vector. If there are N ($N > 1$) observations, the update process changes to,

$$\boldsymbol{y}(k\,|k\,) = \boldsymbol{y}(k\,|k-1\,) + \sum_{j=1}^{N} \boldsymbol{i}_j(k) \tag{22}$$

$$\boldsymbol{Y}(k\,|k\,) = \boldsymbol{Y}(k\,|k-1\,) + \sum_{j=1}^{N} \boldsymbol{I}_j(k) \tag{23}$$

where j is the number of observations. Fig. 5 shows the flowchart of the information filter.

B. INFORMATION FILTER ALGORITHM FOR SHEARER POSITIONING

In this study, the information filter is used to integrate the velocity observation and position observation to improve the shearer positioning accuracy.

It is assumed that the initialization state has no error, that is, $\boldsymbol{X}(0)=[0\ 0\ 0\ 0\ 0\ 0\ 0\ 0\ 0]^{T}$. When the INS is stationary, multiple groups of the INS data are collected, defined as $\boldsymbol{X'}_i$ ($i = 1, 2, \ldots$). The initialization value of $\boldsymbol{P}$ is $\boldsymbol{P}(0)=\mathrm{E}[(\boldsymbol{X'}_i\text{-}\boldsymbol{X}(0))(\boldsymbol{X'}_i\text{-}\boldsymbol{X}(0))^{T}]$, where $\mathrm{E}(\cdot)$ is the mathematical expectation. On the premise of knowing $\boldsymbol{X}(0)$ and $\boldsymbol{P}(0)$, the initialization values of $\boldsymbol{Y}$ and $\boldsymbol{y}$ can be obtained according to Eqs. (16) and (17).

The state vector ($\boldsymbol{X}$), state transition matrix ($\boldsymbol{F}$), and state noise covariance matrix ($\boldsymbol{Q}$) in the information filter are given as (24).

$$\begin{aligned} \boldsymbol{X} &= [\delta L\ \delta\lambda\ \delta h\ \delta V_E\ \delta V_N\ \delta V_U\ \delta\phi_E\ \delta\phi_N\ \delta\phi_U]^{T} \\ \boldsymbol{Q} &= \mathrm{E}[\boldsymbol{W}(i)\boldsymbol{W}(j)^{T}]\,(i=j) \quad \boldsymbol{F} = exp(\boldsymbol{A}T_s) \end{aligned} \tag{24}$$

There are two observations in this study: the velocity observation and the position observation. The observation vector ($\boldsymbol{Z_V}$), observation transition matrix ($\boldsymbol{H_V}$), and observation noise covariance matrix ($\boldsymbol{R_V}$) of the velocity observation are given by Eq. (25). The observation vector ($\boldsymbol{Z_P}$), observation transition matrix ($\boldsymbol{H_P}$), and observation noise covariance matrix ($\boldsymbol{R_P}$) of the position observation are given by Eq. (26).

$$\begin{aligned} \boldsymbol{Z_V} &= \begin{bmatrix} \delta V_{OE} \\ \delta V_{ON} \\ \delta V_{OU} \end{bmatrix} \boldsymbol{H_V} = \begin{bmatrix} 0&0&0&1&0&0&0&0&0 \\ 0&0&0&0&1&0&0&0&0 \\ 0&0&0&0&0&1&0&0&0 \end{bmatrix} \\ \boldsymbol{R_V} &= \mathrm{E}[\boldsymbol{V_V}(i)\boldsymbol{V_V}(j)^{T}](i=j) \end{aligned} \tag{25}$$

$$\begin{aligned} \boldsymbol{Z_P} &= \begin{bmatrix} \delta L_P \\ \delta\lambda_P \\ \delta h_P \end{bmatrix} \boldsymbol{H_P} = \begin{bmatrix} 1&0&0&0&0&0&0&0&0 \\ 0&1&0&0&0&0&0&0&0 \\ 0&0&1&0&0&0&0&0&0 \end{bmatrix} \\ \boldsymbol{R_P} &= \mathrm{E}[\boldsymbol{V_P}(i)\boldsymbol{V_P}(j)^{T}](i=j) \end{aligned} \tag{26}$$

According to the vectors and matrixes in (24), (25), and (26), the estimated error is obtained based on the information filter algorithm. The flowchart of the information filter algorithm for shearer positioning is shown in Fig. 6. The estimated error is used to correct the INS error. Then, the dead reckoning algorithm is applied to calculate the shearer position as (27).

$$\boldsymbol{P}_{\boldsymbol{i}}^{\boldsymbol{n}} = \boldsymbol{P}_{\boldsymbol{i-1}}^{\boldsymbol{n}} + \boldsymbol{C}_{\boldsymbol{b}}^{\boldsymbol{n}^*}[0 \quad v \quad 0]^{T} dt \tag{27}$$

where $\boldsymbol{P}_{\boldsymbol{i}}^{\boldsymbol{n}}$ and $\boldsymbol{P}_{\boldsymbol{i-1}}^{\boldsymbol{n}}$ are the shearer position at time i and $i-1$ in the ENU coordinate system, respectively; $\boldsymbol{C}_{\mathrm{b}}^{\mathrm{n}^*}$ is the new DCM which consists of corrected attitude angles; v is the velocity value measured by the axial encoder; dt is the sampling time between i and $i-1$.

$$\boldsymbol{C}_{\boldsymbol{b}}^{\boldsymbol{n}} = \begin{bmatrix} \cos\gamma\cos\varphi + \sin\gamma\sin\theta\sin\varphi & \cos\theta\sin\varphi & \sin\gamma\cos\varphi - \cos\gamma\sin\theta\sin\varphi \\ -\cos\gamma\sin\varphi + \sin\gamma\sin\theta\cos\varphi & \cos\theta\cos\varphi & -\sin\gamma\sin\varphi - \cos\gamma\sin\theta\cos\varphi \\ -\sin\gamma\cos\theta & \sin\theta & \cos\gamma\cos\theta \end{bmatrix} \tag{8}$$

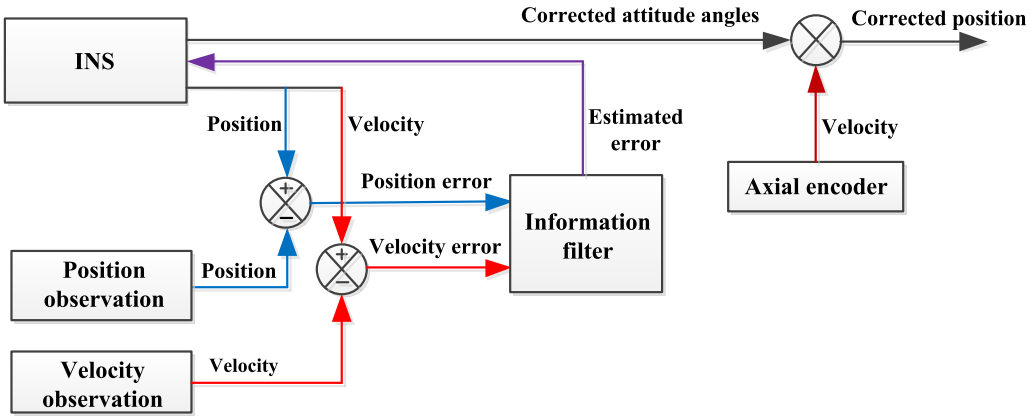

FIGURE 6. The flowchart of the information filter algorithm for shearer positioning.

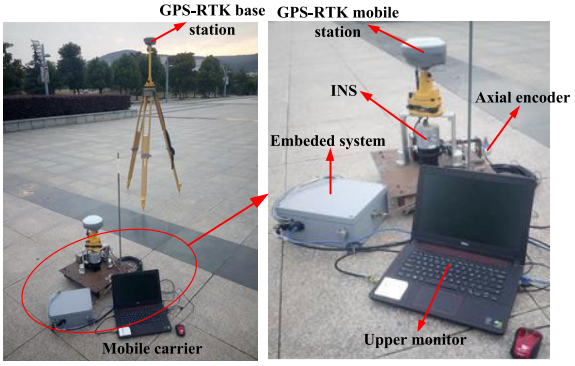

FIGURE 7. The diagram of the experiment site and the experiment device.

TABLE 1. The sensor specifications of INS accelerometer and gyroscope.

Parameter	Accelerometers	Gyroscopes
Range	10g	490°/s
Random walk	0.07 m/s/√hr	0.8 °/√hr
Bias instability	50 ug	0.05 °/hr
Non-linearity	< 0.03 %	< 0.005 %
Scale factor stability	< 0.06 %	< 0.02 %
Cross-axis alignment error	< 0.05 %	< 0.02 %

VI. EXPERIMENTS

To verify the effectiveness of the information filter algorithm for shearer positioning, an experiment with a mobile carrier was conducted as shown in Fig. 7. The INS from ADVANCED NAVIGATION COMPANY was installed in the center of the mobile carrier, and Table 1 shows the sensor specifications of INS accelerometer and gyroscope. The axial encoder was connected to the wheel of the mobile carrier. The resolution of axial encoder was 1/65536. The Global Positioning System – Real Time Kinematic (GPS-RTK) technology was used to evaluate the positioning accuracy, whose dynamic accuracy in the plane was less than 2 cm. The GPS-RTK mobile station was installed on the mobile carrier, and the GPS-RTK base station was fixed on an arbitrary point in the experiment site. The trajectory measured by the GPS-RTK mobile station was considered as the true trajectory of the mobile carrier. The mobile carrier moved four cutting cycles with about 1.5 h at a velocity of 0.1-0.2 m/s in the experiment, and the mobile carrier moved along an approximately straight line during each cutting cycle. It needs special explanation that because the experiment could not really simulate the process of the hydraulic ram pushing the AFC, the advancing displacement was given by the GPS-RTK trajectories between the adjacent cutting cycles. Since the position observation was not available in the first cutting cycle, the data of this cutting cycle was not processed by the information filter algorithm. In addition, because the experiment site is approximately horizontal, the position constraint only existed in the horizontal plane. Therefore, the positioning accuracies in the north and east were discussed in the next.

Prior to four cutting cycles experiment, a calibration experiment was first carried out due to the INS installation error. The mobile carrier moved a short distance at a velocity of 0.4-0.5 m/s. By comparing the measured trajectory and the GPS-RTK trajectory, installation misalignment angle of INS was obtained using two-point method [33]. A comparison of the positioning error with and without calibration in the east and north was shown in Fig. 8. As long as the INS was installed on the mobile carrier, the installation misalignment angle of INS was a definite value, which explained the linear variation of the positioning error without calibration. The maximal error in the east and north decreased from 1.1813 m and 1.6169 m to 0.0932 m and 0.0707 m after the calibration experiment.

Fig. 9 and Fig. 10 show the comparison between the GPS-RTK trajectory and measured trajectory without and with information filter, respectively. Figs. 11, 12, and 13 show the comparison of the heading, pitch, and roll with and without filter, respectively. Fig. 14 shows the variation of the positioning error with and without filter in the east and north. The positioning error without filter in the east and

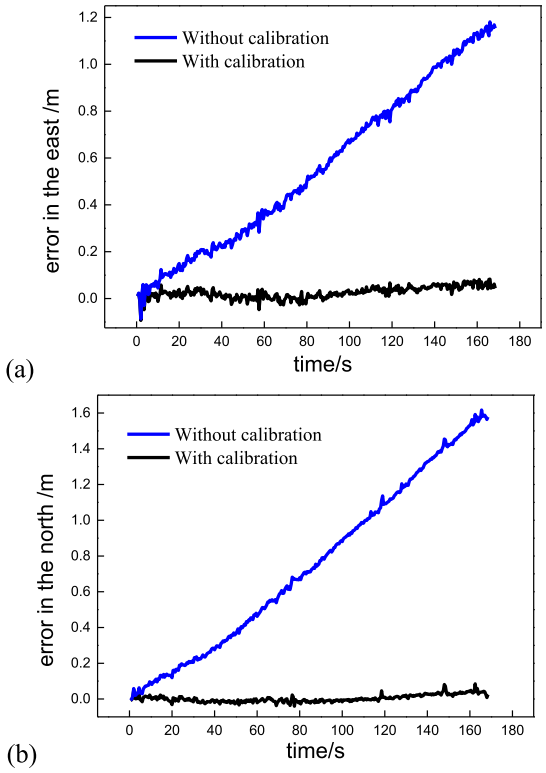

FIGURE 8. Comparison of the positioning error with and without calibration in the (a) east and (b) north.

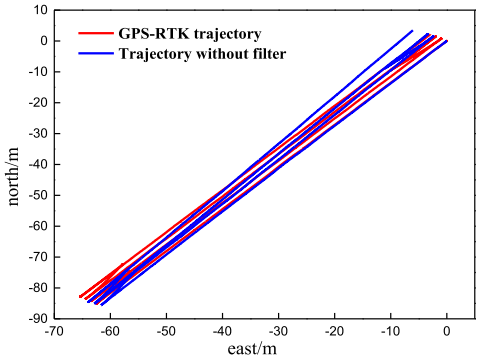

FIGURE 9. Comparison between the GPS-RTK trajectory and the measured trajectory without filter in the east-north plane.

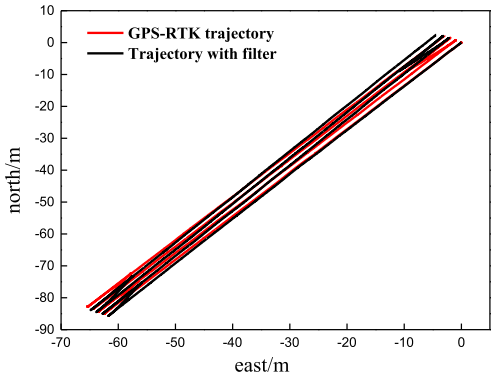

FIGURE 10. Comparison between the GPS-RTK trajectory and the measured trajectory with filter in the east-north plane.

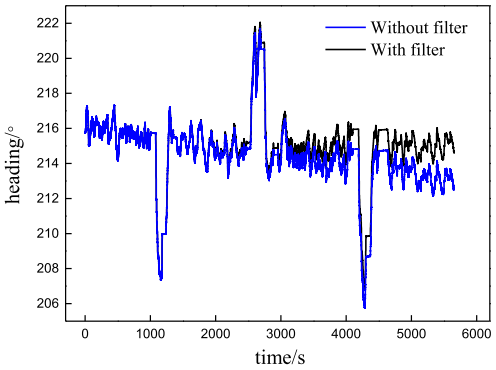

FIGURE 11. Comparison of the heading angle with and without filter.

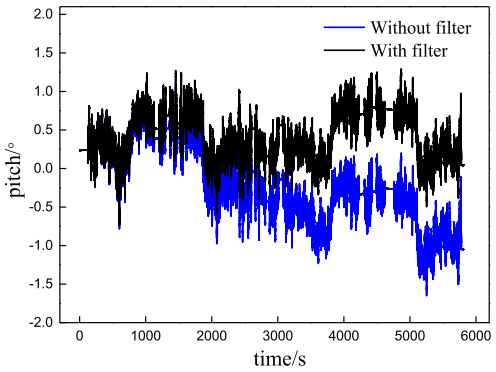

FIGURE 12. Comparison of the pitch angle with and without filter.

north increased with time during the first cutting cycle. In the second, third, and fourth cutting cycles, the variation tendency of the positioning errors without filter were analogous, which first decreased to zero and then increased to maximum. The maximum positioning error without filter occurred at the end of each cutting cycle and the maximum positioning error increased with the number of cutting cycles. As listed in Table 2, the variation values of the positioning error without filter in the east for four cutting cycles were 0.8465 m, 2.1375 m, 3.0874 m and 4.5009 m, and the variation values of the positioning error without filter in the north were 0.6184 m, 1.5411 m, 2.1937 m and 3.1256 m. The error variation values in the east and north increased over the number of cutting cycles, which was caused by the drift of the attitude angles without filter shown in Figs. 11, 12, and 13.

Compared with the attitude angles without information filter, there were no obvious drift for the attitude angles after the information filter, which explained why the measured trajectory with information filter was closer to the GPS-RTK trajectory (Fig. 10) compared with that without information filter (Fig. 9) and the positioning error with filter grew slowly compared with that without information filter (Fig. 14). The positioning error variation values of the measured trajectory with information filter in the east for four cutting cycles were 0.8465 m, 1.9637 m, 1.9497 m and 1.9780 m, and

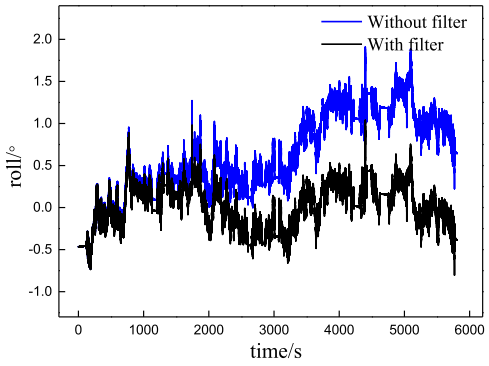

FIGURE 13. Comparison of the roll angle with and without filter.

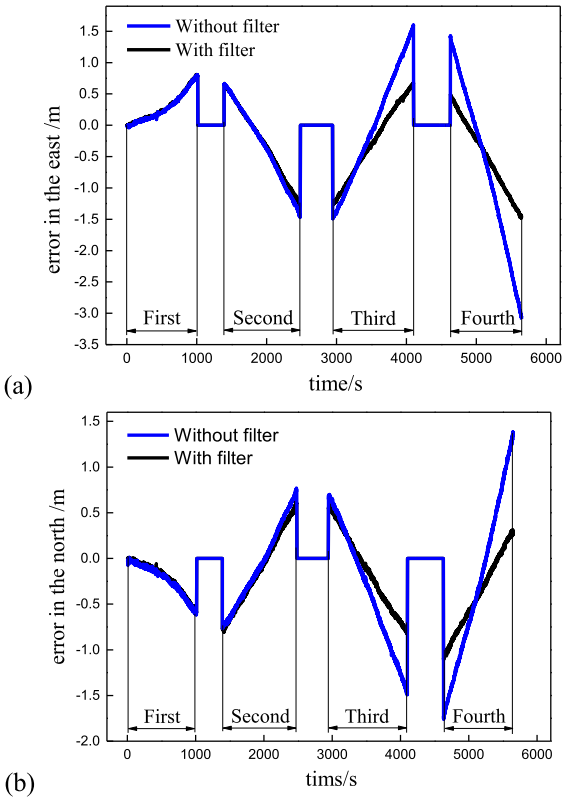

FIGURE 14. Variation of the positioning error with and without filter in the (a) east and (b) north.

the positioning error variation values of the measured trajectory with information filter in the north were 0.6184 m, 1.4223 m, 1.4182 m and 1.4238 m. In the fourth cutting cycle, the shearer positioning accuracy with information filter improved by 56% in the east and 54% in the north. It was noted that the data of the first cutting cycle was not processed by the information filter algorithm. Except for the first cutting cycle, the variation values of the positioning error of other three cutting cycles no longer increased. Due to the filter instability during the early stage, the positioning error variation value of the second cutting cycle increased compared with the first cutting cycle. During the third and fourth cutting cycles, variation values of the positioning error no longer increased, which validated the information filter algorithm restrained the growth of the positioning error. If the high precision positioning can be achieved during the first cutting cycle, the proposed information filter algorithm in this study can be used to maintain high precision positioning during the following cutting cycles. Therefore, how to improve the positioning accuracy during the first cutting cycle is our next research content.

TABLE 2. The positioning error variations (m) in each cutting cycle.

Cutting cycle	East error variation		North error variation	
	Without	With	Without	With
First	0.8465	0.8465	0.6184	0.6184
Second	2.1375	1.9637	1.5411	1.4223
Third	3.0874	1.9497	2.1937	1.4182
Fourth	4.5009	1.9780	3.1256	1.4238

As introduced in Section II, the shearer motion constraints were obtained by analyzing the longwall mining method. In this paper, the experiment parameters including the carrier movement velocity and trajectory were set according to the underground working conditions, and the positioning accuracy with filter improved more than 50%. Compared with the experiment in this paper, the shearer vibration in underground mine is relative larger, which could introduce additional noise in the filter. Therefore, we are now analyzing the shearer vibration spectrum characteristic, which can help us determine the optimal noise variance. In addition, because the coal mine has explosion-proof requirement for equipment, we are designing the explosion-proof circuit and enclosure of the positioning system, and the underground experiment will be performed soon.

VII. CONCLUSION AND PERSPECTIVE

This study used the motion constraints to aid the INS to improve the shearer positioning accuracy. In this study, two constraints of shearer motion on velocity and position were obtained by analyzing the longwall mining method. According to the shearer motion constraints, the velocity observation information and position observation information were modeled, which were used in the observation equations of filter. The information filter algorithm integrating the velocity observation information and position observation information was utilized to improve the shearer positioning accuracy. The experiment result showed that the shearer positioning accuracy after the information filter improved by 56% in the east and 54% in the north. Next, for the problem of low accuracy during the first cutting cycle, the minimum-variance smoothing will be applied to the INS and axial encoder measurements to optimize the positioning trajectory. In addition, we are doing the preparatory work for the underground experiment, including analyzing the shearer vibration spectrum, and designing the explosion-proof circuit and enclosure.

REFERENCES

[1] R. D. Singh, *Principles and Practices of Modern Coal Mining*. Chennai, India: New Age International, 2005.
[2] S. Van Duin, L. Meers, P. Donnelly, and I. Oxley, "Automated bolting and meshing on a continuous miner for roadway development International," *J. Mining Sci. Technol.*, vol. 23, no. 1, pp. 55–61, 2013.
[3] J. Ralston, D. Reid, C. Hargrave, and D. Hainsworth, "Sensing for advancing mining automation capability: A review of underground automation technology development," *Int. J. Mining Sci. Technol.*, vol. 24, no. 3, pp. 305–310, May 2014.
[4] J. C. Ralston, C. O. Hargrave, and M. T. Dunn, "Longwall automation: Trends, challenges and opportunities," *Int. J. Mining Sci. Technol.*, vol. 27, no. 5, pp. 733–739, Sep. 2017.
[5] J. Wang and Z. Huang, "The recent technological development of intelligent mining in China," *Engineering*, vol. 3, no. 4, pp. 439–444, Aug. 2017.
[6] . A. Li, S. Hao, S. Wang, Z. Ge, and S. Ge, "Experimental study on shearer positioning method based on SINS and encoder," (In Chinese), *Coal Sci. Technol.*, vol. 44, no. 4, pp. 95–100, 2016.
[7] X. Fang, J. Zhao, and Y. Hu, "Tests and error analysis of a self-positioning shearer operating at a manless working face," *Mining Sci. Technol.*, vol. 20, no. 1, pp. 53–58, Jan. 2010.
[8] D. C. Reid, J. C. Ralston, M. T. Dunn, and C. O. Hargrave, "A major step forward in continuous miner automation," presented at the 11th Underground Coal Oper., 2011. [Online]. Available: https://ro.uow.edu.au/do/search/
[9] D. Titterton and J. L. Weston, *Strapdown Inertial Navigation Technology*, Edison, NJ, USA: IET, 2004.
[10] M. Ruiz, *Optimization of a Strapdown Inertial Navigation System*. El Paso, TX, USA: The University of Texas at El Paso, 2009.
[11] Q. Fan, W. Li, J. Hui, L. Wu, Z. Yu, W. Yan, and L. Zhou, "Integrated positioning for coal mining machinery in enclosed underground mine based on SINS/WSN," *Sci. World J.*, vol. 2014, Jan. 2014, Art. no. 460415.
[12] J. Xie, Z. Yang, X. Wang, S. Wang, and Q. Zhang, "A joint positioning and attitude solving method for shearer and scraper conveyor under complex conditions," *Math. Problems Eng.*, vol. 2017, Oct. 2017, Art. no. 3793412.
[13] M. T. Dunn, J. P. Thompson, P. B. Reid, and D. C. Reid, "High accuracy inertial navigation for underground mining machinery," in *Proc. IEEE Int. Conf. Autom. Sci. Eng. (CASE)*, Aug. 2012, pp. 1179–1183.
[14] M. Dunn, D. Reid, and J. Ralston, "Control of automated mining machinery using aided inertial navigation," in *Machine Vision and Mechatronics in Practice*. Berlin, Germany: Springer, 2015, pp. 1–9.
[15] S. Ge, Z. Su, A. Li, S. Wang, S. Hao, W. Liu, and L. Meng, "Study on the positioning and orientation of a shearer based on geographic information system," (In Chinese), *J. China Coal Soc.*, vol. 40, no. 11, pp. 2503–2508, 2015.
[16] A. Li, "Research on shearer absolute positioning and attitude technology in mining area," (in Chinese), M.S. thesis, Dept. Mech. Des. Theory, China Univ. Mining Technol., Xuzhou, China, 2015.
[17] B. Zhang, "Research on dynamic accurate positioning method of shearer," (in Chinese), M.S. thesis, Dept. Mech. Des. Theory, China Univ. Mining Technol., Xuzhou, China, 2017.
[18] X. Li, "Theoretical and experimental study on rock cutting in deep mining," (in Chinese), Ph.D. dissertation, Dept. Mech. Des. Theory, China Univ. Mining Technol., Xuzhou, China, 2018.
[19] Y. Ji, T. Ren, P. Wynne, Z. Wan, Z. Ma, and Z. Wang, "A comparative study of dust control practices in chinese and australian longwall coal mines," *Int. J. Mining Sci. Technol.*, vol. 26, no. 2, pp. 199–208, Mar. 2016.
[20] G. A. Einicke, J. C. Ralston, C. O. Hargrave, D. C. Reid, and D. W. Hainsworth, "Longwall mining automation an application of minimum-variance smoothing," *IEEE Control Syst. Mag.*, vol. 28, no. 6, pp. 28–37, Dec. 2008.
[21] S. Hao, S. Wang, R. Malekian, B. Zhang, W. Liu, and Z. Li, "A geometry surveying model and instrument of a scraper conveyor in unmanned longwall mining faces," *IEEE Access*, vol. 5, pp. 4095–4103, 2017.
[22] C. Wang, W. Li, H. Yang, Z. Si, and J. Zhang, "Scraper conveyor shape detection based on dead reckoning," (In Chinese), *J. China Coal Soc.*, vol. 42, no. 8, pp. 2173–2180, 2017.
[23] W. Shibo, Z. Boyuan, W. Shijia, and G. Shirong, "Dynamic precise positioning method of shearer based on closing path optimal estimation model," *IEEE Trans. Autom. Sci. Eng.*, vol. 16, no. 3, pp. 1468–1475, Jul. 2019.
[24] D. Reid, P. Henderson, D. Hainsworth, B. Roberts, A. Chacko, C. Mcleod, and R. Mehl, "Interconnection of landmark compliant longwall mining equipment-shearer communication and functional specification for enhanced horizon control," CSIRO, Canberra, QLD, Australia, Tech. Rep., 2005, pp. 7–35.
[25] P. Liu, B. Wang, Z. Deng, and M. Fu, "INS/DVL/PS tightly coupled underwater navigation method with limited DVL measurements," *IEEE Sensors J.*, vol. 18, no. 7, pp. 2994–3002, Apr. 2018.
[26] H. Nourmohammadi and J. Keighobadi, "Fuzzy adaptive integration scheme for low-cost SINS/GPS navigation system," *Mech. Syst. Signal Process.*, vol. 99, pp. 434–449, Jan. 2018.
[27] Y. Qin, *Kalman Filter and Integrated Navigation* Xi'an, China: Northwestern Polytechnical Univ. Press, 2015.
[28] H. Huang, X. Chen, B. Zhang, and J. Wang, "High accuracy navigation information estimation for inertial system using the multi-model EKF fusing adams explicit formula applied to underwater gliders," *ISA Trans.*, vol. 66, pp. 414–424, Jan. 2017.
[29] Y. Bar-Shalom and X. R. Li, *Estimation and Tracking—Principles, Techniques, and Software*. Norwood, MA, USA: Artech House, 1993.
[30] T. Vercauteren and X. Wang, "Decentralized sigma-point information filters for target tracking in collaborative sensor networks," *IEEE Trans. Signal Process.*, vol. 53, no. 8, pp. 2997–3009, Aug. 2005.
[31] A. G. O. Mutambara, *Decentralized Estimation and Control for Multisensor Systems*. Boca Raton, FL, USA: CRC Press, 1998.
[32] J. Manyika and H. Durrant-Whyte, *Data Fusion and Sensor Management: A Decentralized Information-Theoretic Approach*. Upper Saddle River, NJ, USA: Prentice-Hall, 1995.
[33] B. Zhang, S. Wang, and S. Ge, "Effects of initial alignment error and installation noncoincidence on the shearer positioning accuracy and calibration method," (In Chinese), *J. China Coal Soc.*, vol. 42, no. 3, pp. 789–795, 2017.

SHIJIA WANG was born in Hebei, China, in 1993. He is currently pursuing the Ph.D. degree with the School of Mechanical Design and Theory, China University of Mining and Technology.

His research interests include mining machinery and intelligent mining equipment.

SHIBO WANG was born in Hebei, China, in 1979. He received the Ph.D. degree from the School of Mechanical Design and Theory, China University of Mining and Technology, Xuzhou, China, in 2007.

He is currently a Professor with the China University of Mining and Technology. He is the author of more than 40 articles and holds 10 patents. His research interests include tribology and intelligent mining equipment.